RSC Advances

ROYAL SOCIETY OF CHEMISTRY

www.rsc.org/advances

Near infrared laser–heated electrospinning and mechanical properties of poly(ethylene terephthalate)/multi-walled carbon nanotube nanofibers

Eui Rang Lee and Jae Whan Cho*

Department of Organic and Nano System Engineering, Konkuk University, Seoul 143-701, Korea. E-mail: jwcho@konkuk.ac.kr

Abstract

We report a novel laser-heated electrospinning of poly(ethylene terephthalate) (PET) nanofibers including multi-walled carbon nanotubes (MWNTs) for enhanced mechanical properties. Laser-heated electrospinning was carried out by irradiating the fluid jet stream with a near-infrared laser during electrospinning of a PET/MWNT solution. The laser-heated electrospun nanofibers exhibited a smaller diameter than the electrospun nanofibers without laser heating, and significantly enhanced mechanical properties. The breaking stress and modulus values were higher than those of the electrospun nanofibers without laser heating, and the highest values were obtained at a laser power density of 2.5 W/cm^2. This enhancement in the mechanical properties of nanofibers is ascribed to the increased orientation of both the MWNTs and PET chains along the nanofiber axis, as shown in the polarized Raman spectroscopy measurements. The orientation of the MWNTs due to laser heating was more dominant than the orientation of the PET chains. However, the laser-heated electrospun nanofibers did not show any crystalline peaks in the X-ray diffraction measurements. Laser-heated electrospinning has significant potential for generating carbon nanotube-including nanofibers with smaller diameters and enhanced mechanical properties.

† Electronic supplementary information (ESI) available: Fig. S1–S3.

1. Introduction

Electrospinning has received significant attention because it is an easy and simple method for obtaining continuous nanofibers. Electrospun nanofibers have many advantages over micro-sized melt-spun and solution-spun fibers, including very small fiber diameters, large specific surface areas, high porosities, and high flexibility. However, the weak mechanical properties of electrospun nanofibers have limited their applications in the fields of textiles, filters, tissue engineering, wound dressing, protective materials, and energy applications [1–7]. The relatively weak mechanical properties of electrospun nanofibers are ascribed to the low crystallinity and low molecular orientation formed during electrospinning [8], as compared to those of conventional fibers prepared by melt-spinning and solution-spinning. To overcome these problems, many researchers have developed a variety of electrospinning techniques and investigated the structures and morphologies of the electrospun nanofibers from both theoretical and experimental perspectives [9, 10]. Carbon nanomaterials, such as carbon nanotubes (CNTs) and graphene, have been also used as filler to reinforce the nanofibers [11–15]. Two critical factors such as dispersion and alignment of carbon nanotubes should be solved in order to exploit the intrinsic properties of carbon nanotubes as mechanical reinforcing filler in polymer matrix. However, poor dispersion and alignment of carbon nanomaterials in the polymer matrix has impeded improvement of the mechanical properties of the nanofibers despite the excellent mechanical properties of carbon nanomaterials [16]. Therefore, enhancement of the mechanical properties of nanofibers remains a challenge.

This study reports laser-heated electrospinning, which is defined as electrospinning of a CNT/polymer solution with a near-infrared (NIR) laser irradiating the fluid jet stream just

below the spinneret. The CNTs exhibit photothermal properties because of their localized surface plasmon resonance during laser irradiation [17, 18]. CNTs have a high capacity for converting absorbed light to heat energy and strong absorbance over a wider wavelength range than metal nanoparticles [19, 20]. Accordingly, the laser focused on the fluid jet stream during electrospinning locally heats the CNTs because of the photothermal effects of CNTs dispersed in the polymer solution [21]. Therefore, the laser-heated fluid stream flows at a higher speed because of the decreased viscosity caused by the elevated temperature of the jet stream. As a result, laser heating of the fluid stream during the electrospinning process may effectively enhance the orientation of polymer chains and CNTs. In addition, the local heating of CNTs in the laser heated electrospinning has an excellent advantage against high-temperature solution electrospinning where the heating is not controlled locally over the nanofibers. So the laser heated electrospinning is very effective for controlling the orientation of CNTs in the CNT composite nanofibers, whereas the high-temperature solution electrospinning is used to obtain the nanofibers from the polymer solution such as polyethylene solution with relatively poor solubility [22].

Herein, we report novel laser-heated electrospinning to obtain high-performance poly(ethylene terephthalate) (PET) nanofibers that include multi-walled carbon nanotubes (MWNTs). The PET fibers have long been one of the most important fibers in both textiles and industrial applications [23–26]. The mechanical properties of the laser-heated electrospun PET/MWNT nanofibers are investigated in terms of the orientation of the PET chains and MWNTs as well as PET crystallization.

2. Experimental

2.1. Materials

PET (I.V. = 0.64 dL/g) chips were supplied from Hyosung Co. (Korea), and MWNTs with a

diameter of 10–15 nm, average length of about 20 μm, and purity of 95% were purchased from Hanwha Nanotech (Korea). Trifluoroacetic acid (TFA) and dichloromethane (DCM) were purchased from Sigma Aldrich Korea.

2.2. Preparation of nanofibers by laser-heated electrospinning

A PET/MWNT solution in a mixed solvent of TFA/DCM (7:3 v/v) was prepared for electrospinning. First, the MWNTs (0.001 g) were dissolved in the TFA/DCM mixture (7.9 mL), and the solution was sonicated for 2 h using a horn-type sonicator. Then, PET chips (2 g) were added to the MWNT solution after being dried in an oven, and the mixture was stirred for 48 h. Homogeneously dispersed PET/MWNT solutions were obtained after sonication in a bath-type sonicator for 30 min (Figure S1). The resultant PET/MWNT solutions contained 0.5 wt% MWNTs in PET.

The PET/MWNT solutions were electrospun at room temperature using an electrospinning setup (NNC-ESR100, NanoNC, Korea) with NIR-laser (808 nm wavelength) irradiation of the fluid jet stream just below the spinneret (Figure 1a). With the irradiation of the NIR laser with a spot size of 0.8 x 0.5 cm^2, the fluid jet stream of the PET/MWNT solution was heated very rapidly, and different laser intensity densities of 1.25, 2.5, and 3.75 W/cm^2 were used. The applied voltage for electrospinning was 15 kV, and the tip-to-collector distance and volumetric flow rate were 15 cm and 0.9 μL/min, respectively.

2.3. Characterization

Wide-angle X-ray scattering (WAXS) measurements were carried out using a New D8-Advance diffractometer (Bruker-AXS) with a CuK_α X-ray source. The surface morphology of the electrospun nanofibers was observed using field emission scanning electron microscopy (FE-SEM, S-4300SE, Hitachi). Morphology of the MWNTs in the electrospun nanofibers

was observed by transmission electron microscopy (TEM, JEM 2100F, JEOL). Differential scanning calorimetry (DSC) measurements were performed using a model 2010 thermal analyzer (TA Instruments, DuPont) at a heating rate of 10 °C/min under a flow of nitrogen gas. The mechanical properties of the nanofiber webs were measured at an elongation rate of 15 mm/min at room temperature using a tensile tester (Instron 4468). Samples with an average thickness of 100 μm, length of 50 mm, and width of 4 mm were used for the tensile test. At least five samples were tested and their average values were used. Polarized Raman spectroscopy measurements were carried out to evaluate the orientation of the PET chains and MWNTs in nanofibers webs that were drawn at a draw ratio of 2.0 at 95 °C. The Raman spectra were recorded at room temperature with the incident and back-scattered light parallel to the drawing direction of the nanofiber webs using a HORIBA Jobin Yvon LabRAM ARAMIS instrument (France). The Raman spectrometer was equipped with a He-Ne laser beam with a 632.8 nm wavelength and 1 mW excitation light source. For the polarized Raman spectra, the nanofiber webs were rotated 0° and 90° in order to orient the polarization of the laser beam parallel and perpendicular, respectively, to the drawing direction of the nanofiber webs [27, 28]. The intensities of the Raman beam with parallel and perpendicular polarization to the fiber drawing direction are referred to as I_0 and I_{90}, respectively.

3. Results and Discussion

Laser-heated electrospinning of the PET/MWNT solution was performed at laser power densities of 0, 1.25, 2.5, and 3.75 W/cm^2 using an NIR laser with a wavelength of 808 nm. Polymer solutions with a PET concentration of 15 wt% in a mixed solvent of TFA/DCM that included 0.5 wt% MWNTs were used for electrospinning. Figure 1a shows a schematic of the laser-heated electrospinning set-up used in this study. For laser-heated electrospinning, the NIR laser was focused onto the fluid jet stream of the PET/MWNT solution, causing rapid

heating of the spinning fluids because of the photothermal properties resulting from the localized surface plasmon resonance of MWNTs. The photothermal properties of the fluid stream are strongly dependent on the MWNT content and laser power density. Figure 1b exhibits the photothermal properties of the MWNT powders measured at laser power densities of 0.5, 1.0, and 1.5 W/cm^2. The surface temperature of the MWNT powders increased rapidly with laser irradiation time and increased with increased laser power density. When the laser power was off, the temperature decayed very quickly. From Figure 1b, it can be considered that due to the photothermal properties of MWNTs, the PET/MWNT solution in the laser heated electrospinning could be rapidly heated by laser irradiation, which reduced the viscosity of the polymer solution. As a result, the electrospinning speed of the fluid jet stream increased with increased laser power density while the diameter of the electrospun nanofibers decreased. Figure 1c shows photothermal images of the MWNTs powders over time under irradiation with lasers with different power densities.

Figure 2a shows SEM images of electrospun PET and PET/MWNT nanofibers without laser heating and electrospun PET/MWNT nanofibers with laser heating at different laser power densities. All the nanofibers have uniform surfaces regardless of laser heating. However, the diameter of the laser-heated electrospun nanofibers decreased significantly relative to those of the electrospun PET and PET/MWNT nanofibers without laser heating. The average diameters of the nanofibers electrospun under irradiation with different laser power densities are shown in Figure 2b. The pure PET and PET/MWNT nanofibers without laser heating have average diameters of 1.5 and 1.1 μm, respectively; however, the electrospun PET/MWNT nanofibers that were laser-heated at 3.75 W/cm^2 have an average diameter of 0.67 μm, which is less than half the diameter of the pure PET nanofibers. This indicates that very thin nanofibers can be obtained using laser-heated electrospinning.

Figure 3 shows the mechanical properties of pure PET and PET/MWNT nanofibers, as

obtained from the tensile stress–strain curves (Figure S2). From this figure, it is evident that the mechanical properties, such as breaking stress and modulus, are significantly affected by the laser power density. The nanofibers electrospun at a laser power density of 2.5 W/cm^2 had the highest breaking stress and modulus values of 4.21 and 92.9 MPa, respectively, whereas the breaking stress and modulus values of the electrospun PET/MWNT nanofibers without laser heating were 3.24 and 78.8 MPa, respectively. The nanofibers prepared at a higher laser power density of 3.75 W/cm^2 exhibited lower breaking stress and modulus values than those prepared at a laser power density of 2.5 W/cm^2. This may be because electrospinning at a higher laser power density induces molecular slippage and rapid solidification in laser heating and cooling, respectively and thus prevents molecular orientation. The laser-heated electrospun PET/MWNT nanofibers also show significantly higher elongation-at-break values than the electrospun nanofibers without laser heating, although the electrospun pure PET nanofibers show the highest elongation-at-break value. These enhanced mechanical properties of the laser-heated electrospun nanofibers may result from crystallization of the PET chains and improved orientation of the PET chains and MWNTs of the nanofibers during the electrospinning process.

To investigate the crystallization behavior of the laser-heated electrospun nanofibers, WAXS and DSC measurements were carried out. Figure 4a shows the WAXS diffractograms of the pure PET and PET/MWNT nanofibers with and without laser heating. All the diffraction curves of the samples feature a broad amorphous halo without any X-ray diffraction peaks to indicate crystals; this suggests that the electrospun nanofibers do not crystallize during the electrospinning process regardless of laser heating [16, 29]. Figure 4b shows DSC curves of the nanofibers measured during heating at 10 °C/min. All the samples show similar crystallization patterns, that is, glass transition temperatures near 77 °C, cold crystallization temperatures at about 118–123 °C, and melting temperatures at about 256–

260 °C [30, 31]. These crystallization behaviors reflect that all the electrospun nanofibers are in the amorphous state, which corresponds with the results of the WAXS measurements. On the other hand, the laser-heated electrospun nanofibers have slightly lower cold crystallization and melting temperatures than the nanofibers that were electrospun without laser heating. Also, as the laser power density increased, the cold crystallization and melting temperatures also tended to decrease slightly. The decreased crystallization and melting temperatures of laser heated electrospun nanofibers may result from the decreased diameter of the nanofibers. It has been explained to be due to the entropy jump corresponding to the polymer's melting resulting from lower chain entanglement in the nanofibers than in the polymer bulk [32]. In addition, the polymer crystallization of laser heated electrospun PET/MWNT nanofibers may occur in relatively stressed state, compared to polymer crystallization of electrospun nanofibers without laser heating. Similar results were reported in our previous study: Polymer crystallization of CNT composite fibers in a stressed or elongated state leads to less perfect crystallization [33, 34], and this is in contrast to crystallization in a free state where the MWNTs act as nucleating agents for crystallization [29, 35]. Therefore the lower cold crystallization and melting temperatures in this study is considered to result from the polymer crystallization in the stressed state as well as decreased diameter due to the laser heating.

The orientation of the PET chains and MWNTs in the laser-heated electrospun nanofibers was evaluated using polarized Raman spectroscopy. Figure 5 shows polarized Raman spectra of the drawn webs of nanofibers that were electrospun with and without laser heating. Prior to polarized Raman spectroscopic analysis, the nanofiber webs were drawn at a draw ratio of 2.0 at 95 °C because polarized Raman spectroscopy cannot deduce the orientation of the polymer chains and MWNTs in undrawn nanofiber webs. The polarized Raman spectra in Figure 5 show characteristic peaks at 1180, 1340, 1580, and 1614 cm^{-1}. The peaks at 1180 and 1614

cm^{-1} are due to the stretching modes of the C–C bonds and C=C bonds of the PET chains, respectively [36], and the peaks at 1340 and 1580cm^{-1} are due to the D and G modes of the MWNTs, which correspond to the sp^3 and sp^2 carbon atoms, respectively [37]. The I_0 and I_{90} of the characteristic peaks of the Raman spectra for the drawn nanofiber webs with and without laser heating are clearly different, whereas they are very similar for the undrawn nanofiber webs (Figure S3). The differences between I_0 and I_{90} result from the differences in the orientations of the PET chains and MWNTs. Therefore, the ratio of the peak intensities, i.e., I_0/I_{90}, at 1614 and 1580 cm^{-1} can be used to quantify the orientation of the PET chains and MWNTs, respectively [38, 39]. Figure 6 exhibits the values of I_0/I_{90} for the PET chains and MWNTs as a function of laser power intensity. The value of I_0/I_{90} for the undrawn nanofiber webs is close to 1.0, indicating a lack of orientation; however, the value of I_0/I_{90} for the drawn nanofiber webs increases gradually with increasing laser power intensity in the range of a laser power density of 2.5 W/cm^2 and then drops again with further increase in the laser power density; this occurs for the orientation of both the PET chains and MWNTs. These results indicate that laser heating during electrospinning facilitates the orientation of the MWNTs and PET chains. Interestingly, the increase in the I_0/I_{90} value with increased laser power density is more dominant for the MWNTs than for the PET chains, and, for the MWNTs, a very high value of 3.68 was obtained at a laser power density of 2.5 W/cm^2. This indicates that the MWNTs orient themselves more effectively than the PET chains during laser-heated electrospinning because of the localized heating around the MWNTs. This result corresponds well with the mechanical properties of the nanofibers discussed previously. In addition, TEM images of electrospun nanofibers with and without laser heating were measured as shown in Figure 7. It is clear that TEM images of electrospun PET/MWNT nanofibers with laser heating (Figure 7b-d) show good orientation of MWNT along the nanofiber axis, whereas the electrospun PET/MWNT nanofiber without laser heating (Figure

7a) shows good dispersion but almost random or less orientation of MWNT in the nanofiber. Therefore, the laser-heated electrospinning described in this study has high potential as an effective method for enhancing the mechanical properties of nanofibers.

4. Conclusions

NIR laser–heated electrospinning of PET/MWNT solution resulted in thinner and stronger nanofibers. The laser-heated electrospun nanofibers showed enhanced breaking stress and modulus values than those of the nanofibers that were electrospun without laser heating. The optimal mechanical properties were obtained from nanofibers electrospun at a laser power density of 2.5 W/cm^2. The enhanced mechanical properties of the laser-heated nanofibers were ascribed to the increased degree of orientation of the MWNTs and PET chains along the nanofiber axis, as evidenced by the polarized Raman spectra. The laser-heated electrospinning used in this study effectively generates better orientation of the MWNTs and polymer chains, in particular the MWNTs, in nanofibers.

Acknowledgements: This work was supported by the Basic Science Research Program through the National Research Foundation of Korea (NRF) funded by the Ministry of Education (No. NRF-2014R1A1A2055053).

References

1. Z. M. Huanga, Y. Z. Zhang, M. Kotakic and S. Ramakrishn, *Compos. Sci. Technol.*, 2003, **63**, 2223-2253.

2. D. Li and Y. Xia, *Adv. Mater.*, 2004, **16**, 1151-1170.

3. T. J. Sill and H. von Recum, *Biomaterials*, 2008, **29**, 1989-2006.

4. C. Chang, V. H. Tran, J. Wang, Y. K. Fuh and Liwei Lin, *Nano Lett.*, 2010, **10**, 726-731.

5. S. W. Choi, S. M. Jo, W. S. Lee and Y. R. Kim, *Adv. Mater.*, 2003, **15**, 2027-2032.

6. R. Gopal, S. Kaur, Z. Ma, C. Chan, S. Ramakrishna and T. Matsuura, *J. Membrane Sci.*, 2006, **281**, 581-586.

7. H. Wang, C. Chu, R. Cai, S. Jiang, L. Zhai, J. Lu, X. Li and S. Jiang, *RSC Adv*., 2015, **5**, 53550-53558.

8. S. F. Fennessey and R. J. Farris, *Polymer*, 2004, **45**, 4217-4225.

9. J. Lee and Y. Deng, *Macromol. Res.*, 2012, **20**, 76-83.

10. C. L. He, Z. M. Huang and X. J. Han, *J. Biomed. Mater. Res. A*, 2009, **89**, 80-95.

11. H. J. Yoo, H. H. Kim, J. W. Cho and Y. H. Kim, *Surf. Interface Anal.*, 2012, **44**, 405-411.

12. L. D. Tijing, C. H. Park, S. J. Kang, A. Amarjargal, T. H. Kim, H. R. Pant, H. J. Kim, D. H. Lee and C. S. Kim, *Appl. Surf. Sci.*, 2013, **264**, 453-458.

13. H. J. Yoo, S. S. Mahapatra and J. W. Cho, *J. Phys. Chem. C*, 2014, **118**, 10408-10415.

14. Q. Bao, H. Zhang, J. X. Yang, S. Wang, D. Y. Tang, R. Jose, S. Ramakrishna, C. T. Lim and K. P. Loh, *Adv. Funct. Mater*., 2010, **20**, 782-791.

15. J. H. Kim, M. Kataoka, Y. C. Jung, Y. I. Ko, K. Fujisawa, T. Hayashi, Y. A. Kim and M. Endo, *ACS Appl. Mater. Inter.*, 2013, **5**, 4150-4154.

16. S. Mazinani, A. Ajji and C. Dubois, *J. Polym. Sci., Part B: Polym. Phys*., 2010, **48**, 2052-2064.

17. D. Boldor, N. M. Gerbo, W. T. Monroe, J. H. Palmer, Z. Li and A. S. Biris, *Chem. Mater.*, 2008, **20**, 4011-4016.

18. X. Shen, C. Viney , C. Wang and J. Q. Lu, *Adv. Funct. Mater.*, 2014, **24**, 77-85.

19. A. O. Govorov and H. H. Richardson, *Nano Today*, 2007, **2**, 30-38.

20. Z. M. Markovic, L. M. Harhaji-Trajkovic, B. M. Todorovic-Markovic, D. P. Kepić, K. M. Arsikin, S. P. Jovanović, A. C. Pantovic, M. D. Dramićanin and V. S. Trajkovic, *Biomaterials*, 2011, **32**, 1121-1129.

21. M. Takasaki, K. Hara, Y. Ohkoshi, T. Fujii, H. Shimizu and M. Saito, *Polym. Eng. Sci.*, 2014, **54**, 2605-2609.

22. S. R. Givens, K. H. Gardner, J. F. Rabolt and D. B. Chase, *Macromolecules*, 2007, **40**, 608-610.

23. B. Veleirinho and J.A. Lopes-da-Silva, *Process Biochem.*, 2009, **44**, 353-356.

24. M. Ignatova, T. Yovcheva, A. Viraneva, G. Mekishev, N. Manolova and I. Rashkov, *Eur. Polym. J.*, 2008, **44**, 1962-1967.

25. I. S. Chronakis, B. Milosevic, A. Frenot and L. Ye, *Macromolecules*, 2006, **39**, 357-361.

26. M. G. McKee, G. L. Wilkes, R. H. Colby and T. E. Long, *Macromolecules*, 2004, **37**, 1760-1767.

27. L. M. Bellan and H. G. Craighead, *Polymer*, 2008, **49**, 3125-3129.

28. M. V. Kakade, S. Givens, K. Gardner, K. H. Lee, D. B. Chase and J. F. Rabolt, *J. Am. Chem. Soc*., 2007, **129**, 2777-2782.

29. H. Chen, Z. Liu and P. Cebe, *Polymer*, 2009, **50**, 872-880.

30. Z. G. Wang, B. S. Hsiao, B. B. Sauer and W. G. Kampert, *Polymer*, 1999, **40**, 4615-4627.

31. Z. Li, G. Luo, F. Wei and Y. Huang, *Compos. Sci. Technol.*, 2006, **66**, 1022-1029.

32. A. Arinstein, Y. Liu, M. Rafailovich and E. Zussman, *A Lett. J. Exploring The Frontiers of Phys.*, 2011, **93**, 46001-p1-p6.

33. D. H. Fu, Y. H. Zhan, N. Yan and H. S. Xia, *Express Polym. Lett.*, 2015, **9**, 597-607.

34. H. J. Yoo, K. H. Kim, S. K. Yadav and J. W. Cho, *Compos. Sci. Technol*., 2012, **72**, 1834-1840.

35. Y. Sun and C. He, *RSC Adv*., 2013, **3**, 2219-2226.

36. R. Paquin, M. H. Limage and P. Colomban, *J. Raman Spectrosc.*, 2007, **38,** 1097-1105.

37. G. S. Duesberg, I. Loa, M. Burghard, K. Syassen, and S. Roth, Phys. Rev Lett., 2000, **85**, 5436-5439.

38. P. Pötschke, H. Brünig, A. Janke, D. Fischer and D. Jehnichen, *Polymer*, 2005, **46**, 10355-10363.

39. N. Romyen, S. Thongyai and P. Praserthdam, *J. Appl. Polym. Sci.*, 2012, **123**, 3070-3475.

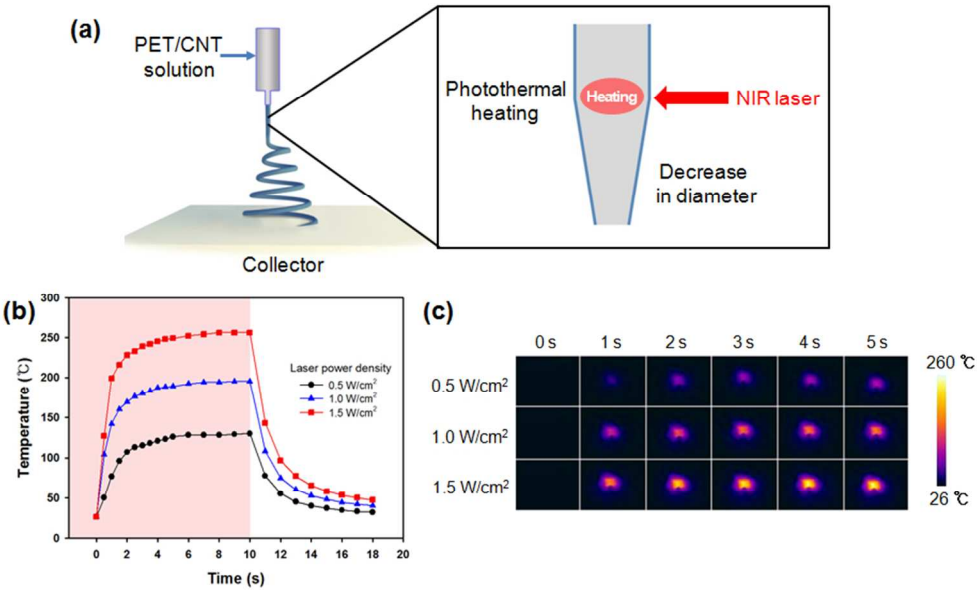

Figure 1. (a) Scheme of the NIR laser–heated electrospinning set-up, (b) surface temperature of MWNTs over time with laser irradiation at different laser power densities, and (c) photothermal images after laser irradiation of the MWNTs at different laser power densities.
330x195mm (72 x 72 DPI)

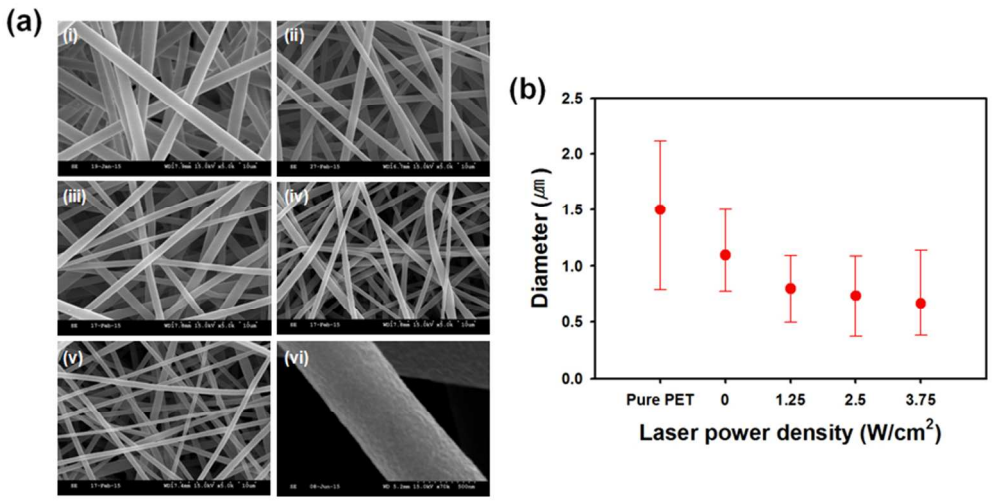

Figure 2. (a) SEM images of electrospun (i) PET and (ii) PET/MWNT nanofiber webs without laser heating and electrospun PET/MWNT nanofiber webs that were laser-heated at laser power densities of (iii) 1.25, (iv) 2.5, and (v, vi) 3.75 W/cm2. (b) Diameters of the nanofibers generated at different laser power densities.
335x171mm (72 x 72 DPI)

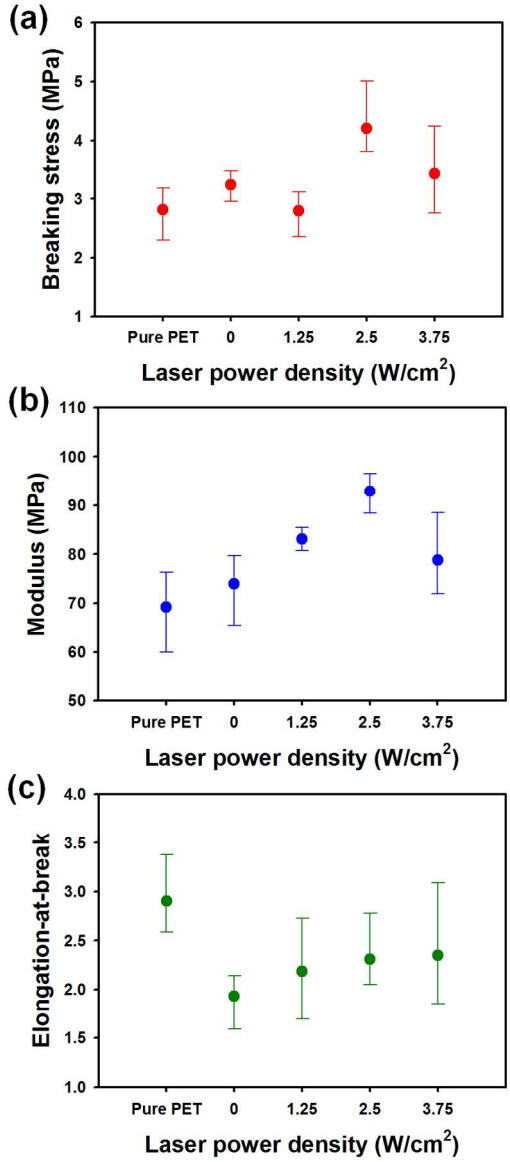

Figure 3. (a) Breaking stress, (b) modulus, and (c) elongation-at-break of electrospun pure PET and PET/MWNT nanofiber webs without laser heating and electrospun PET/MWNT nanofiber webs that were laser-heated at different laser power densities.
168x367mm (150 x 150 DPI)

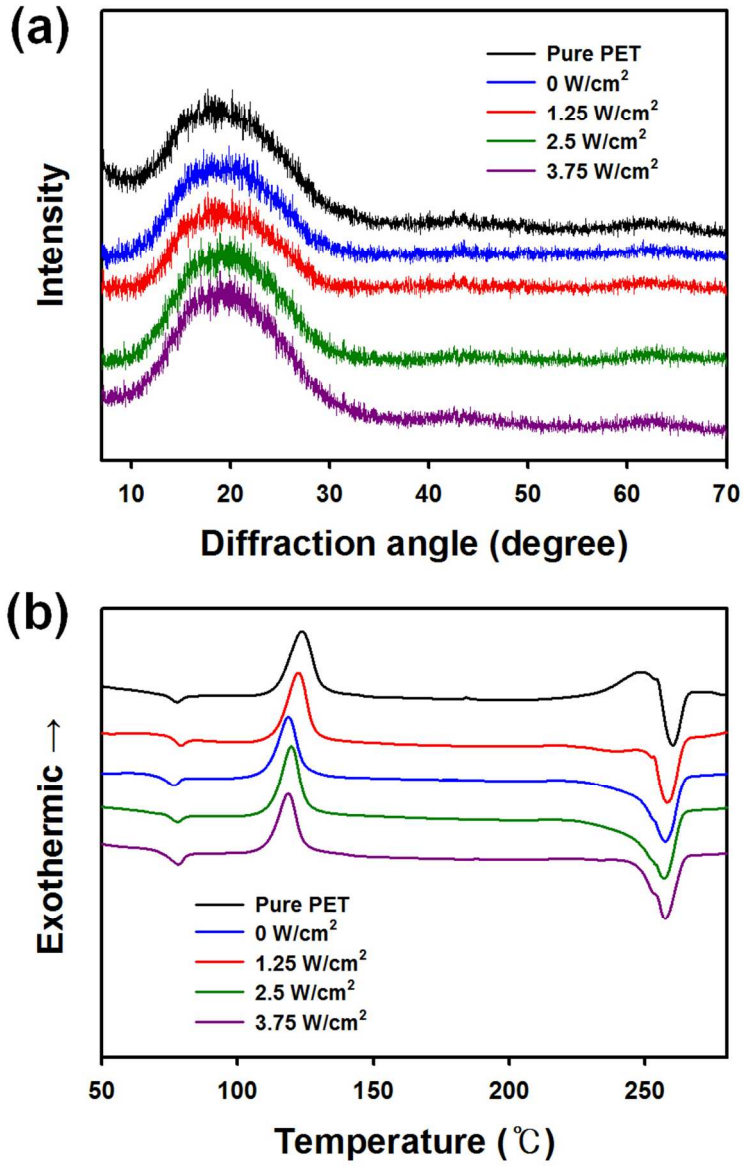

Figure 4. (a) Wide-angle X-ray diffractograms and (b) DSC thermograms of pure PET and PET/MWNT nanofiber webs without laser heating and electrospun PET/MWNT nanofiber webs that were laser-heated at different laser power densities.
153x239mm (150 x 150 DPI)

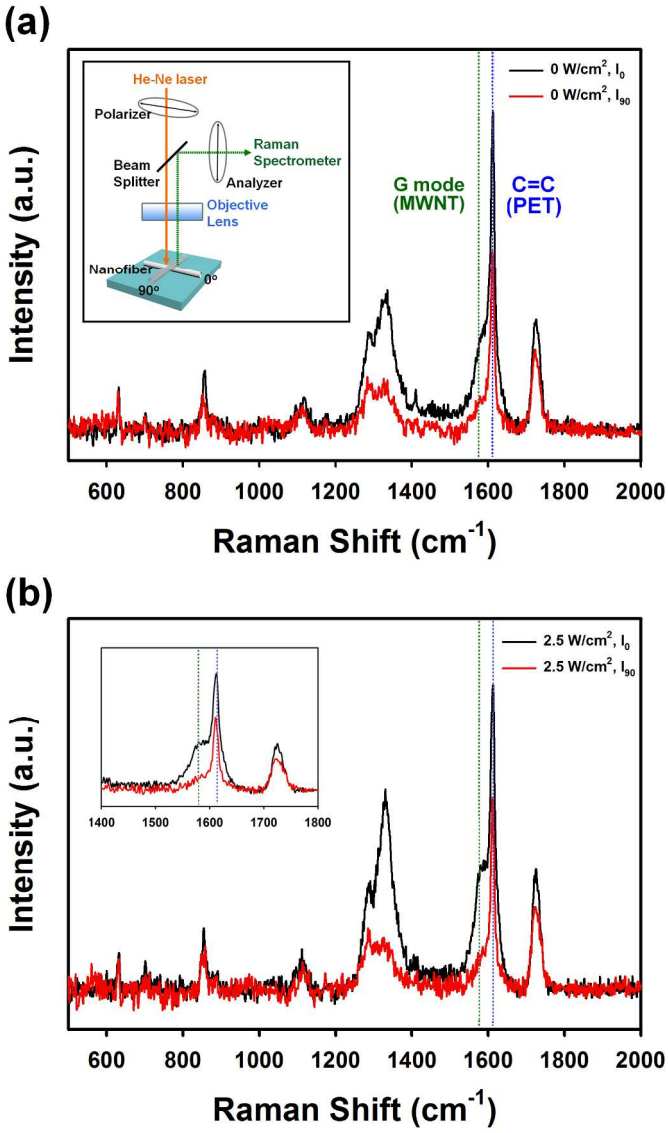

Figure 5. I_0 and I_{90} polarized Raman spectra of (a) electrospun PET/MWNT nanofiber webs without laser heating and (b) electrospun PET/MWNT nanofiber webs that were laser-heated at a laser power density of 2.5 W/cm2.
147x262mm (300 x 300 DPI)

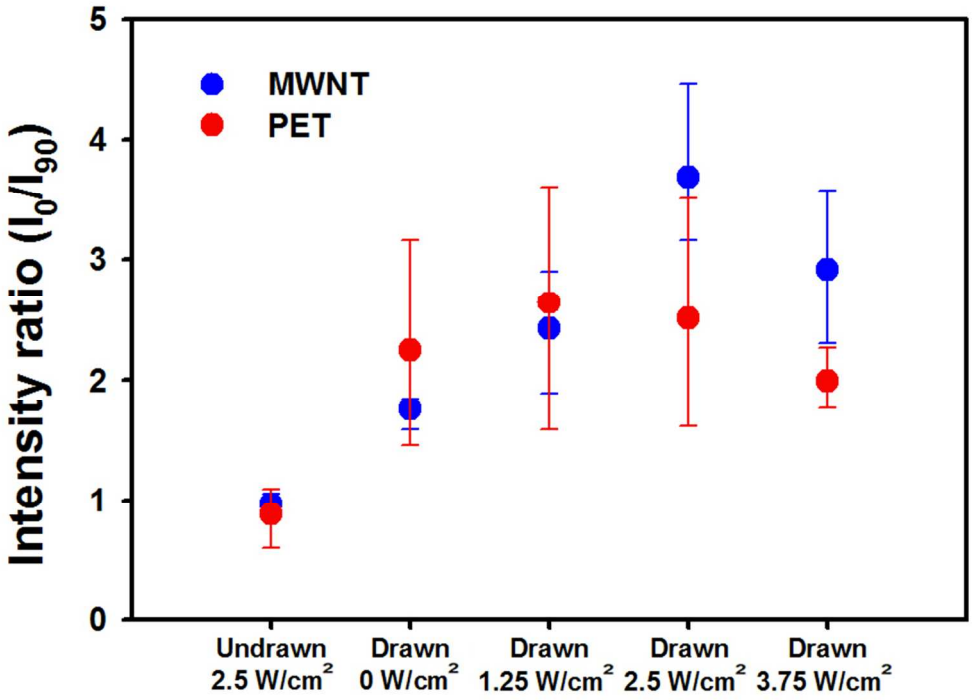

Figure 6. I_0/I_{90} values for undrawn and drawn PET/MWNT nanofiber webs without and with laser heating at different laser power densities.
149x108mm (150 x 150 DPI)

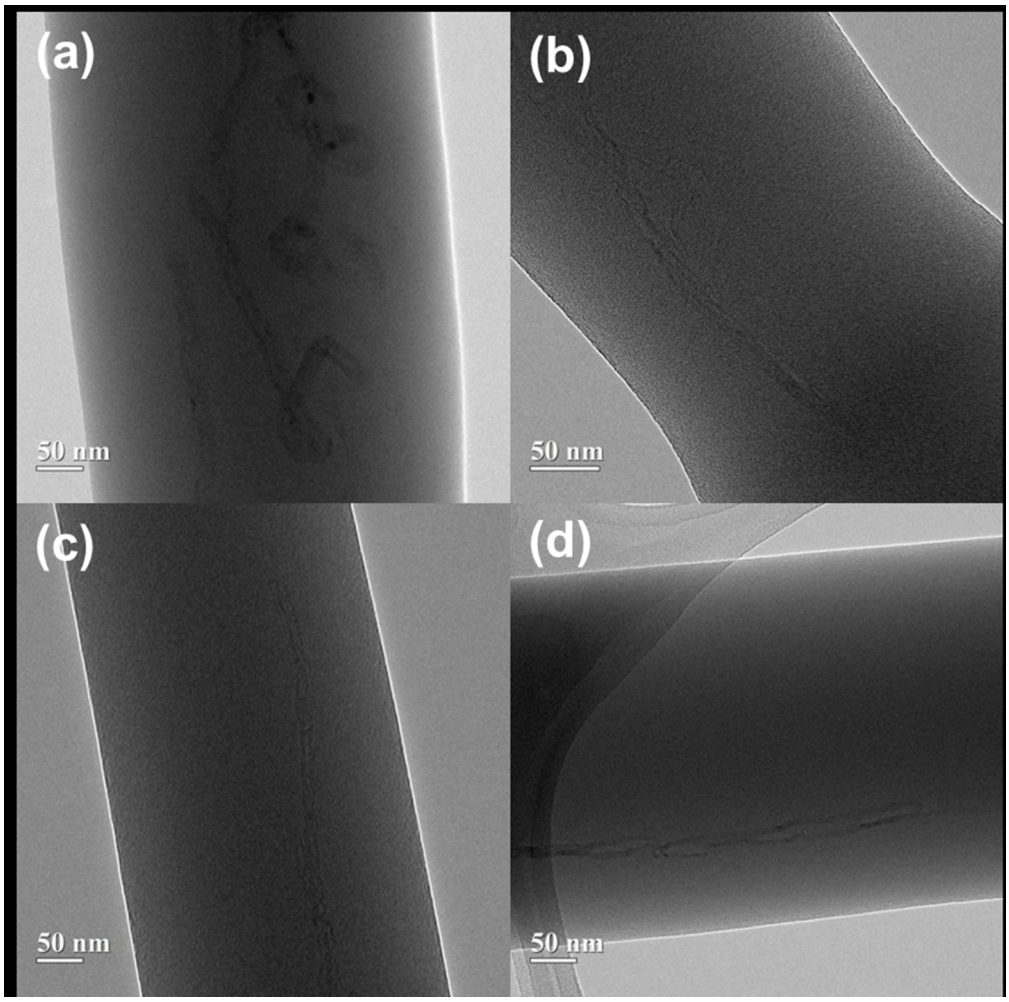

Figure 7. TEM images of electrospun PET/MWNT nanofibers (a) without laser heating and (b-d) with laser heating at the laser power densities of (b) 1.25, (c) 2.5, and (d) 3.75 W/cm$^{2.}$
142x140mm (150 x 150 DPI)

Table of Contents

The carbon nanotube-including poly(ethylene terephthalate) nanofibers with enhanced mechanical properties were electrospun by using a near infrared laser-heated electrospinning.